Introduction to HBC Channel Models:

Table 1: HBC communication pathways considered for FEM analysis.

Channel Model	Path	Description
CM1	Aorta to Chest	Pair of electrodes attached to the ascending aorta and left side of the chest.
CM2	Aorta to Heart	Pair of electrodes attached to the ascending aorta and left ventricle.
CM3	Left Kidney to Back	Pair of electrodes attached to the left kidney and lower back (left side).
CM4	Left Renal Vein to Back	Pair of electrodes attached to the left renal veins and lower back (left side).
CM5	Left Renal Vein to Kidney	Pair of electrodes attached to the left renal veins and left kidney.

Three-dimensional human anatomy software (BioDigital) was used to determine the major organ and tissue structures between the transmitter the receiver electrodes. The five communication pathways are visualized in Figure 1 to Figure 5.

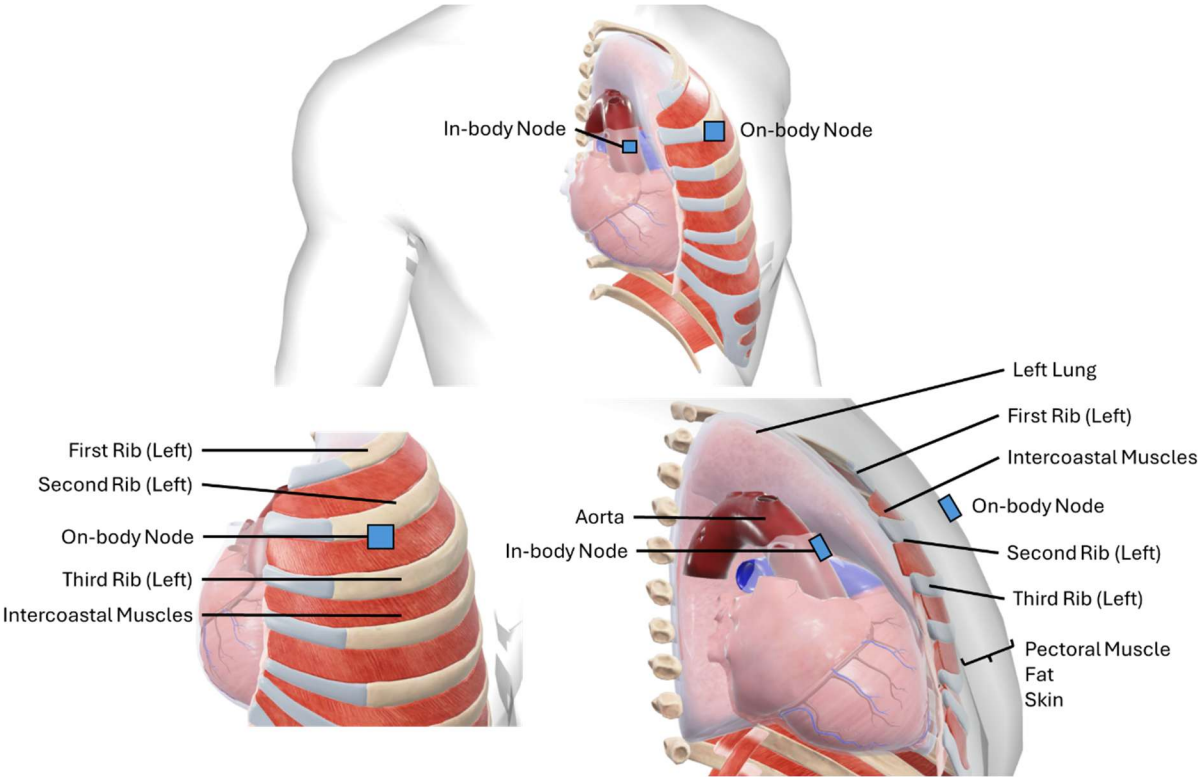

Figure 1: Proposed Communication Pathway, CM1 (top), Front-view (bottom-left) and Side-view (bottom-right).

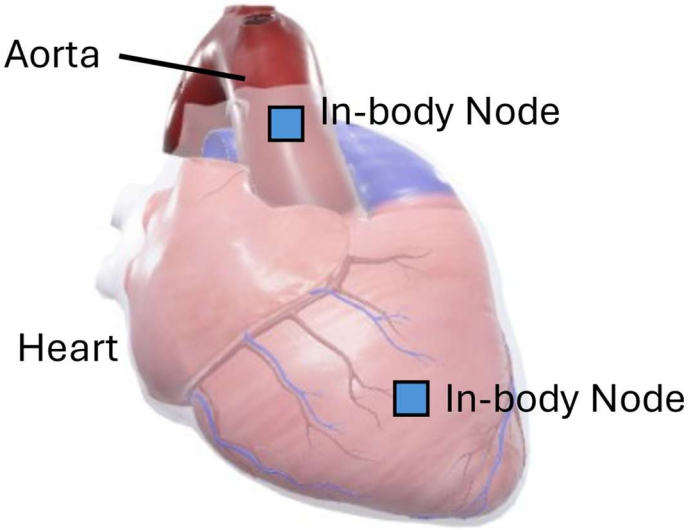

Figure 2: Proposed Communication Pathway, CM2.

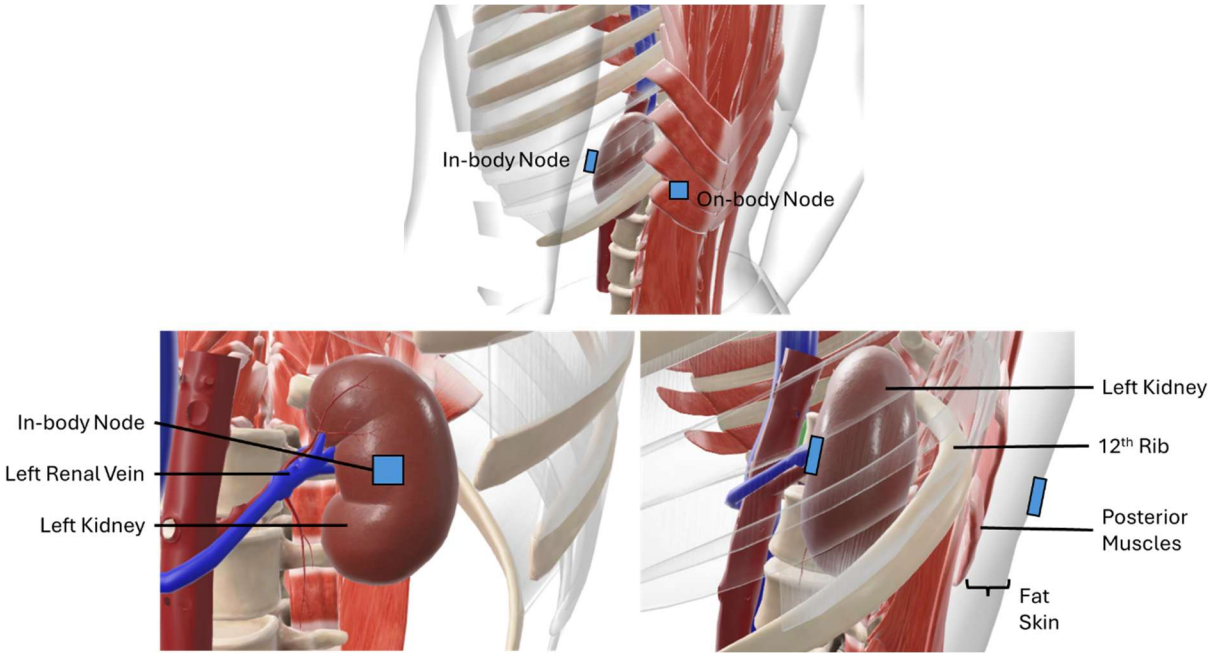

Figure 3: Proposed Communication Pathway, CM3 (top), Front-view (bottom-left) and Side-view (bottom-right).

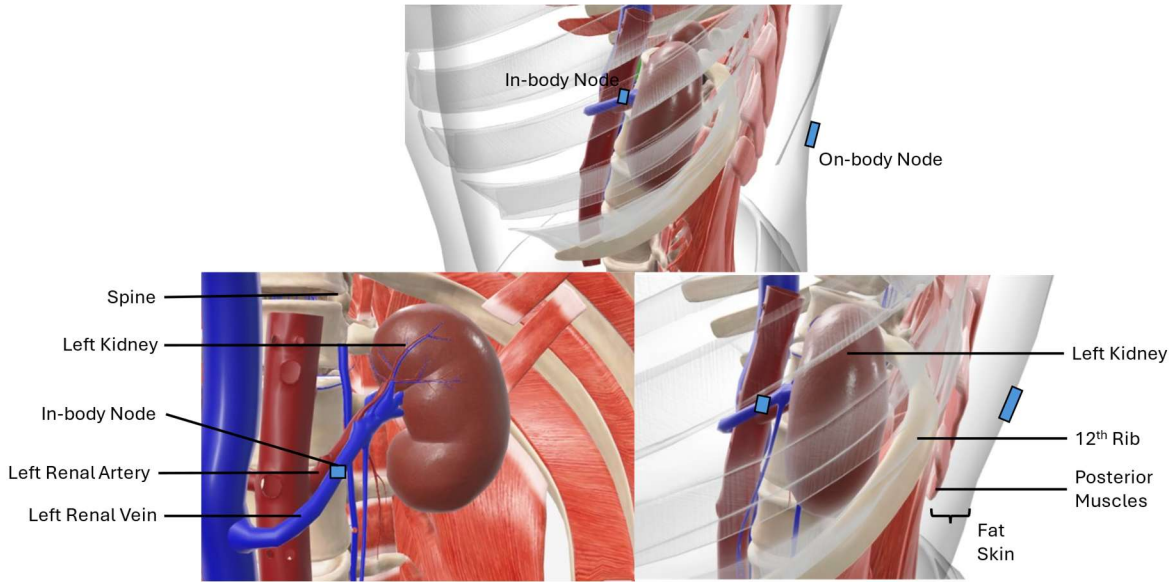

Figure 4: Proposed Communication Pathway, CM4 (top), Front-view (bottom-left) and Side-view (bottom-right).

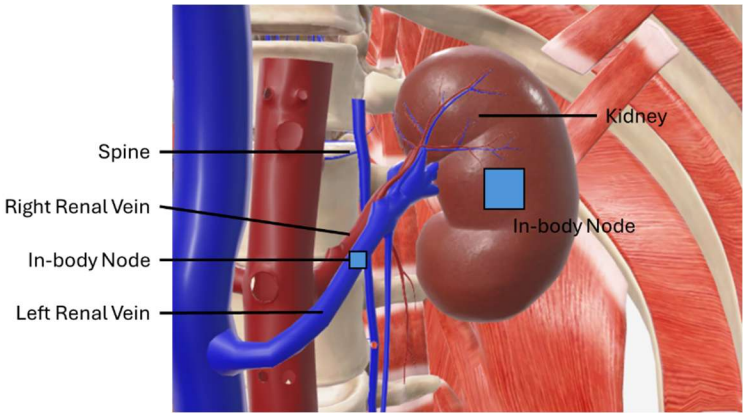

Figure 5: Proposed Communication Pathway, CM5 (top), Front-view (bottom-left) and Side-view (bottom-right).

Geometry and Channel Model Parameters

For FEM analysis of the various HBC pathways outlined in Table 1 the geometries and parameters used to construct these models are outlined in the following sections. Since galvanic coupling is used, there is a pair of electrodes at the transmitting and receiving site. At the transmitter, one of the electrodes are used as a ground electrode while the other acts a current source. At the receiver side, both electrodes are configured as terminals and are used to simulate electric coupling about the ground terminal. Additionally, a load resistance of 1kΩ was placed between the receiver electrode pair. A schematic of this setup is shown in Figure 6 below.

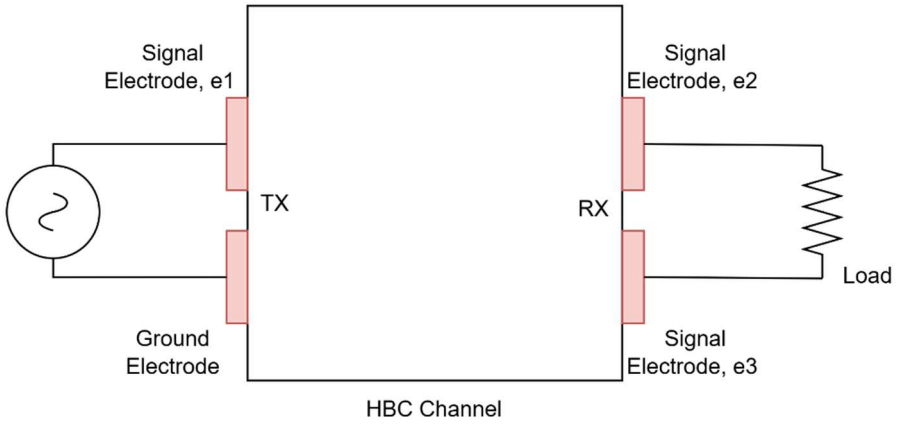

Figure 6: Arrangement of Electrodes for Galvanic HBC.

The electrodes are assumed to be square in shape with negligible thickness. The size of the electrodes however was restricted to those used in patient care and other HBC experimental setups (Lobodzinski 2010; Callejon et al. 2013). The spacing between electrode pairs, z_{space} were restricted to 2mm. Additionally, the relative permittivity and conductivity of all biological structures (tissue, organs or fluids) required by the models were

computed from the complex permittivity expressions from (Sasaki, Wake, and Watanabe 2014).

CM1: Aorta to Chest Model

The geometry considered for this study consisted of a cylindrical structure modelling the aorta and five (5) rectangular layers modelling the human chest. Each layer represented a different tissue/structure between the transmitter and receiver electrodes observed in Figure 1. These are, the lung tissue, cancellous rib bone/intercostal muscle, pectoralis muscle, fat, and skin. The cross-section of the chest model is L_{chest} x W_{ches} . The thicknesses of the organs modelled follow average sizes outlined in various studies.

The model blueprints in Figure 7 and Figure 8 describe how the COMSOL model is constructed along with the various parameters required. The parameters of this model as well its supporting resource(s) where appropriate are summarized in Table 2. Finally, the model blueprints and parameters are used to construct the COMSOL model in Figure 9.

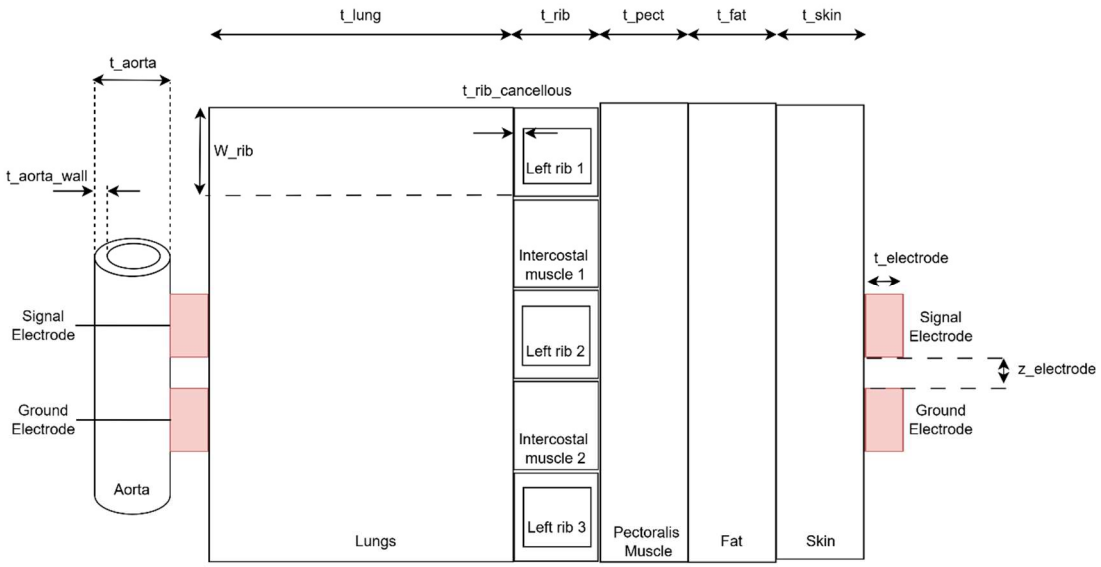

Figure 7: HBC Channel, CM1 Model Blueprint (Side-view).

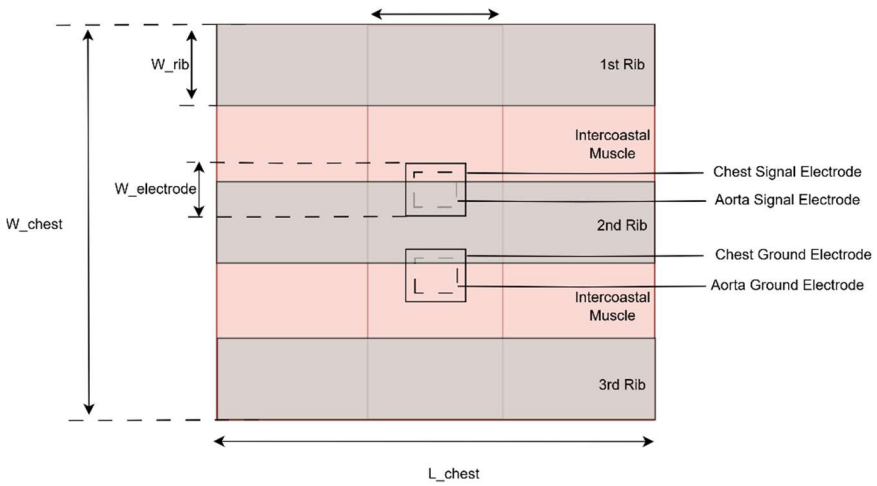

Figure 8: HBC Channel, CM1 Model Blueprint (Front-view).

Table 2: FEM Modelling Parameters for the CM1 channel (Aorta to Chest).

Parameter	Value	Description
t_{aorta}	2.66 [cm]	Average diameter of the ascending aorta (Davis et al. 2013).
$t_{aorta\ wall}$	4 [mm]	Thickness of the aortic walls (Erbel and Eggebrecht 2006).
t_{lung}	8.2 [mm]	Thickness of the left human lung (Chekan et al. 2016).
$t_{rib\_cancellous}$	0.9 [mm]	Thickness of the cancellous bone of the human rib (Holcombe et al. 2019).
t_{rib}	6 [mm]	Thickness of the human rib (Mohr et al. 2007).
t_{pect}	4 [mm]	Thickness of the pectoralis muscle (Hacking and Pacifici 2011).
t_{fat}	5.55 [mm]	Thickness of fat at the chest area (Nösslinger et al. 2022; Störchle et al. 2018).
t_{skin}	6.05 [mm]	Thickness of the skin layer at the chest (Oltulu et al. 2018).
L_{chest}	11 [cm]	Length of CM1 area under study.
W_{chest}	11 [cm]	Width of the CM1 area under study.

$W_{electrode}$	2 [cm]	Aorta electrode size under study.
W_{rib}	11.3 [mm]	Height of the human rib (Mohr et al. 2007).

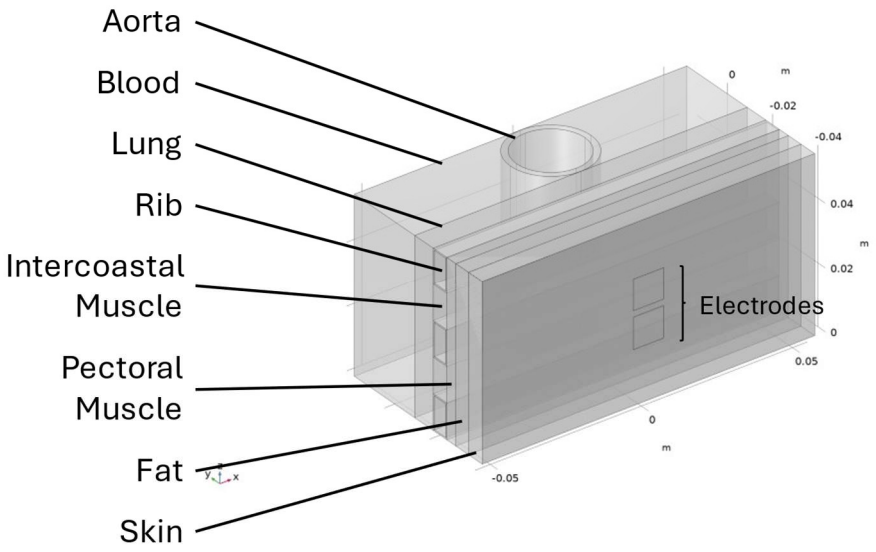

Figure 9: COMSOL Model for the Aorta to Chest Model (CM1).

CM2: Aorta to Heart Model

The geometry considered for this study used spherical and elliptical shapes to model the heart similar to the model presented in (Filippi and Cherubini 2024). A cylinder was used to model the outgoing aorta (refer to Figure 2). The thicknesses of the structures modelled followed average sizes outlined in various studies. The model blueprints in Figure 10 and Figure 11 describe how the COMSOL model is constructed along with the parameters required. The heart and aorta model were placed in a block of blood of dimensions, $L_{model} \times W_{model} \times L_{heart}$ (L x W x H) to model the various tissue and blood vessels around the heart.

The parameters of this model as well its supporting resource(s) where appropriate are summarized in Table 3. Additionally, to ensure the electrodes curve around the aorta and heart the side of the electrode was constructed as an arc. The sector angle was computed using the desired electrode size and the radius of the circular surface. For example, the sector angle used to build the aorta electrodes is given below:

$$\theta = \frac{2W_{electrode}}{t_{aorta}} \quad [1]$$

Finally, the model blueprints and parameters are used to construct the COMSOL model in Figure 9.

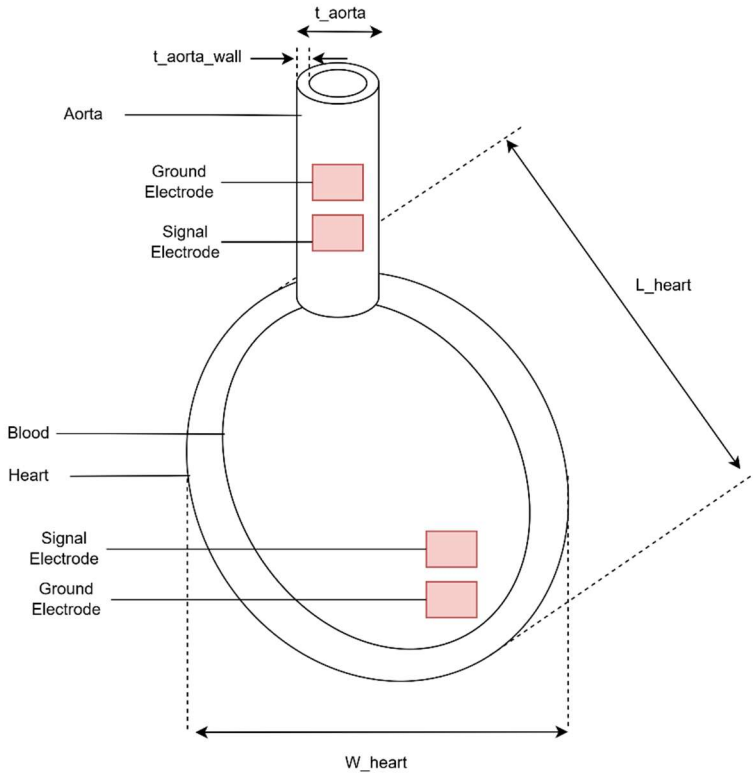

Figure 10: HBC Channel, CM2 Model Blueprint (Front-view).

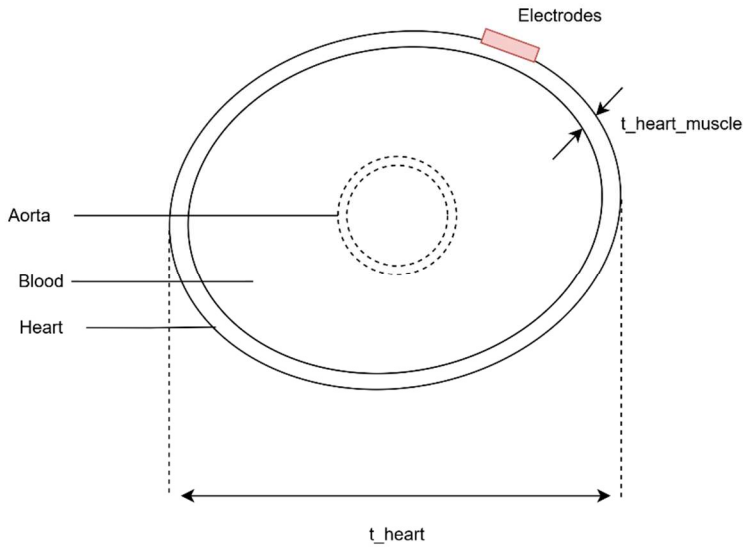

Figure 11: HBC Channel, CM2 Model Blueprint (Side-view).

Table 3: FEM modelling parameters for the aorta to chest channel.

Parameter	Value	Description
t_{aorta}	26.6 [mm]	Average diameter of the ascending aorta (Davis et al. 2013).
$t_{aorta\ wall}$	4 [mm]	Thickness of the aortic walls (Erbel and Eggebrecht 2006).
$t_{heart\ muscle}$	10.6 [mm]	Thickness of the heart muscles (Kawel et al. 2012).
t_{heart}	6 [cm]	Thickness of the human heart (Bianco 2021).
L_{model}	17 [cm]	Length of CM2 area under study.
L_{heart}	12 [cm]	Length of the human heart from base to apex (Bianco 2021).
W_{model}	15 [cm]	Width of CM2 area under study.
W_{heart}	8 [cm]	Width of the human heart (Bianco 2021).
$W_{electrode}$	2 [cm]	Size of the heart electrode.

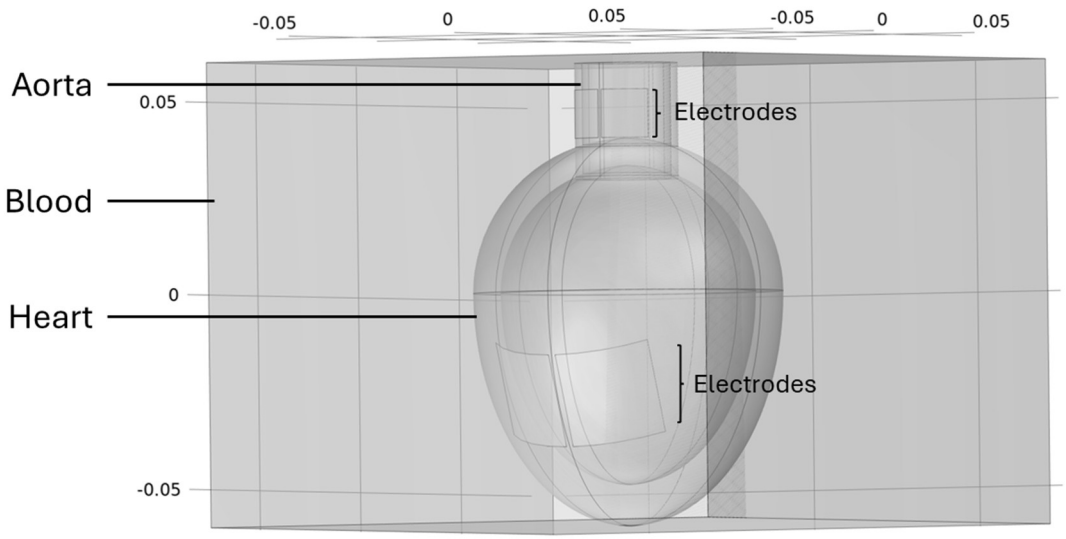

Figure 12: COMSOL Model for the Aorta to Heart Model (CM2).

CM3: Left Kidney to Back

The geometry considered for this study consisted of five (5) rectangular layers modelling the human chest. Each layer represented a different tissue/structure between the transmitter and receiver electrodes observed in Figure 3. These are, the kidney, posterior muscle (iliocostalis and serratus), connective muscle, fat, and skin. The cross-section of the model was denoted by L_{kidney} x W_{back}. The thicknesses of the organs and tissues modelled follow average sizes outlined in various studies.

The model blueprints in Figure 13 and Figure 14 describe how the COMSOL model is constructed along with the various parameters required. The schematic in Figure 15 is used to build the kidney in COMSOL. It utilized two circular arcs (GA and BC), a line segment (AB) and an interpolation curve using points (C, D, E, F, G). The resulting outline (A, B, C, D, E, F, G) was converted to a solid and its internal boundaries were removed to realize the kidney

shape in Figure 15. The parameters of this model as well its supporting resource(s) where appropriate are summarized in Table 4. Finally, the model blueprints and parameters are used to construct the COMSOL model in Figure 9.

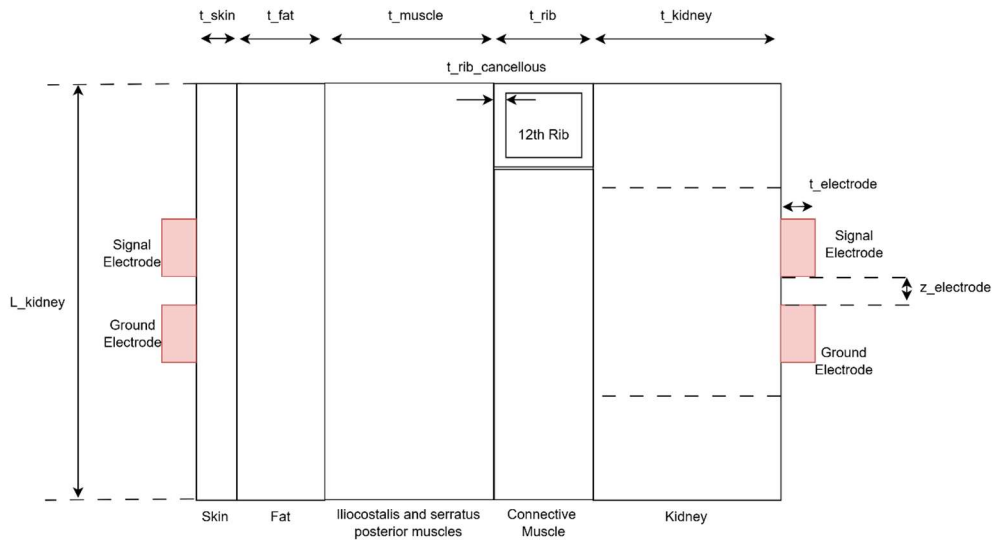

Figure 13: HBC Channel, CM3 Model Blueprint (Side-view).

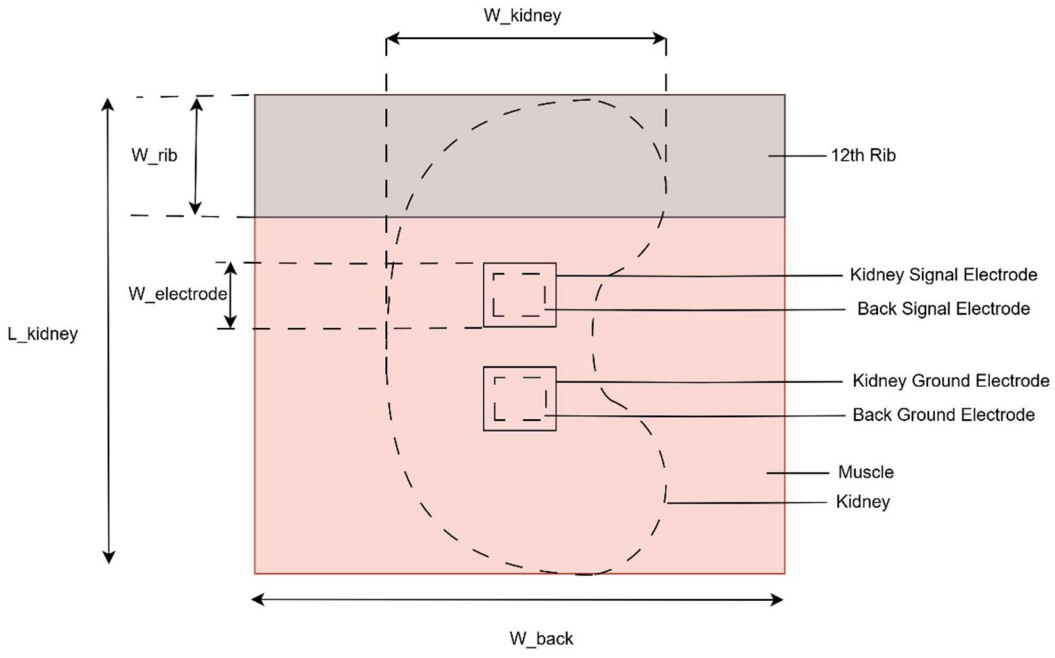

Figure 14: HBC Channel, CM3 Model Blueprint (Front-view).

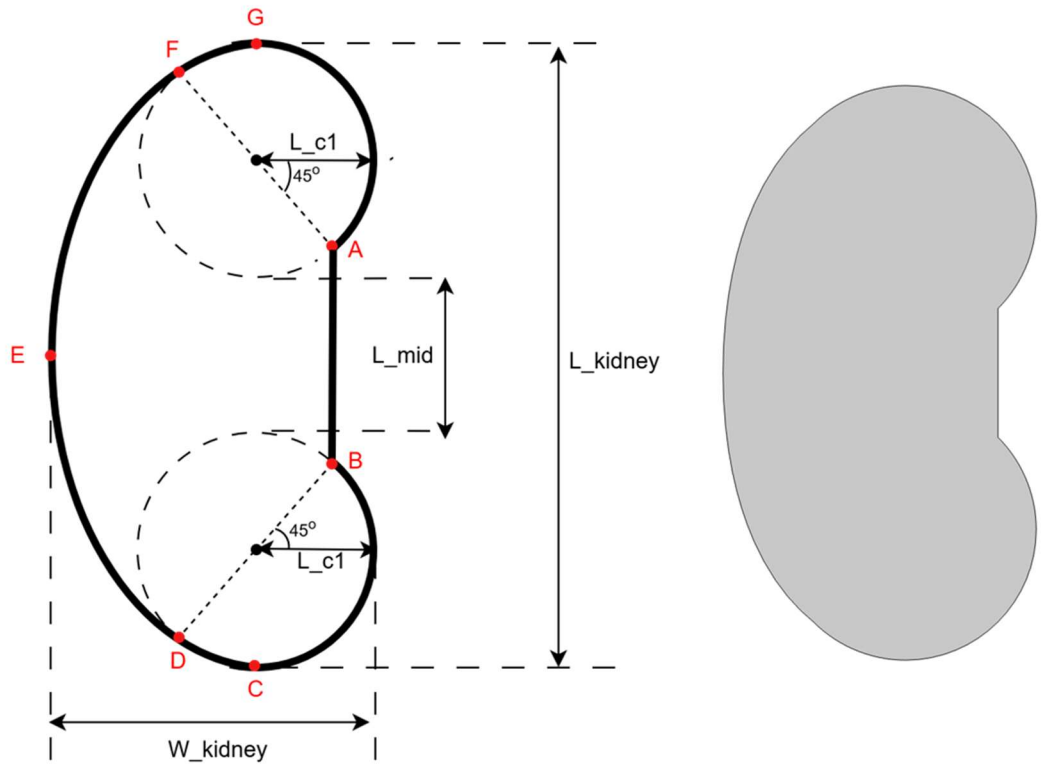

Figure 15: Schematic of Kidney Construction in COMSOL Multiphysics (Left) and the Resulting Kidney Shape (Right).

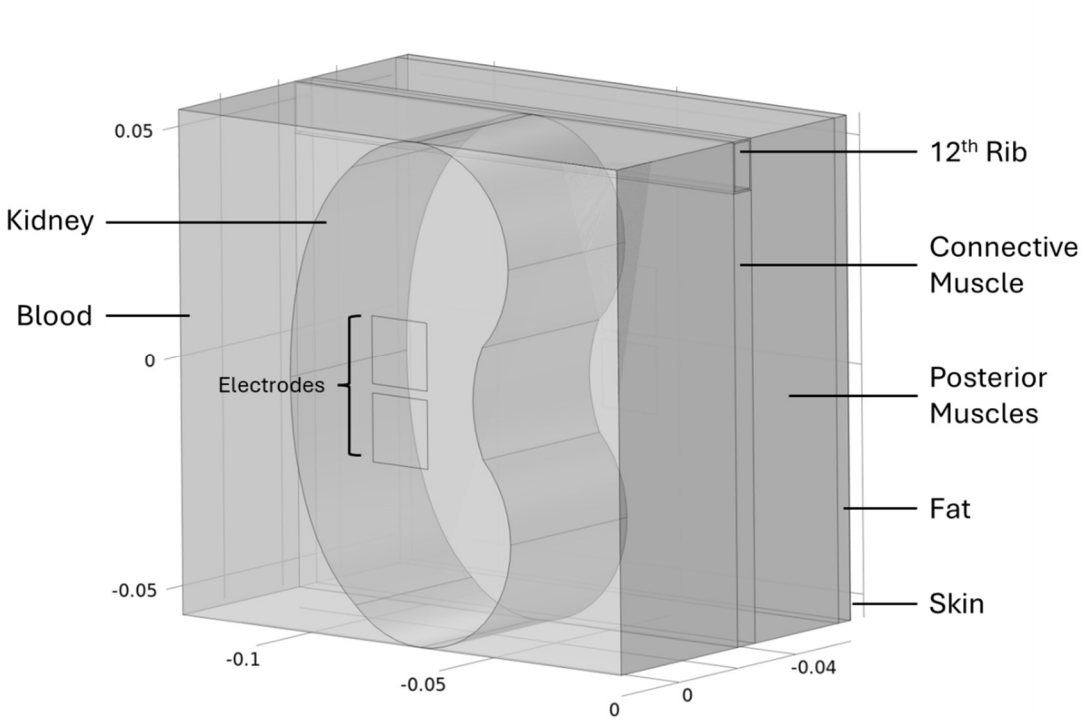

Figure 16: COMSOL Model for the Kidney to Back Model (CM3).

Table 4: FEM Modelling Parameters for the Kidney to Back Channel.

Parameter	Value	Description
t_{kidney}	4 [cm]	Thickness of the left human kidney (Soriano, Penfold, and Leslie 2023).
t_{muscle}	2.87 [cm]	Thickness of the posterior muscles at the back of a human (Miyachi et al. 2022).
t_{fat}	4 [mm]	Thickness of the subcutaneous fat at the posterior trunk of a human (Störchle et al. 2018).
t_{skin}	0.12 [mm]	Thickness of the skin at the posterior trunk of a human (Oltulu et al. 2018).
$t_{rib\_cancellous}$	0.9 [mm]	Thickness of the cancellous bone of the human rib (Holcombe et al. 2019).
t_{rib}	6 [mm]	Thickness of the human rib (Mohr et al. 2007).
L_{mid}	1 [cm]	Chosen for this study.
L_{kidney}	11 [cm]	Length of the human kidney (Soriano, Penfold, and Leslie 2023).
W_{back}	14 [cm]	Width of CM3 area under study.
W_{kidney}	6 [cm]	Width of the human kidney (Soriano, Penfold, and Leslie 2023).
W_{rib}	11.3 [mm]	Width of the human rib (Mohr et al. 2007).
$W_{electrode}$	2 [cm]	Size of the back electrodes for this study.

CM4: Left Renal Vein to Back

The geometry considered for this study consisted of three (4) rectangular layers modelling the skin, fat, muscle/spine and kidney layer. Each layer represented a different tissue/structure between the transmitter and receiver electrodes observed in Figure 4. The muscle/spin layer contains the spine structure, the posterior muscle as well as the 12th rib. The kidney layer rests on the surface of the muscle/spine layer. In this layer, the kidney, renal artery, renal vein, abdominal aorta and inferior vena cava are constructed. The kidney is designed as described in the previous section (refer to Figure 15). The blood vessels are designed using cylinders. The cross-section of the model was denoted by L_{kidney} x W_{model}. The thicknesses of the organs and tissues modelled follow average sizes outlined in various studies.

The model blueprints in Figure 17 and Figure 18 describe how the COMSOL model is constructed along with the various parameters required. The parameters of this model as well its supporting resource(s) where appropriate are summarized in Table 5. Finally, the model blueprints and parameters are used to construct the COMSOL model in Figure 19.

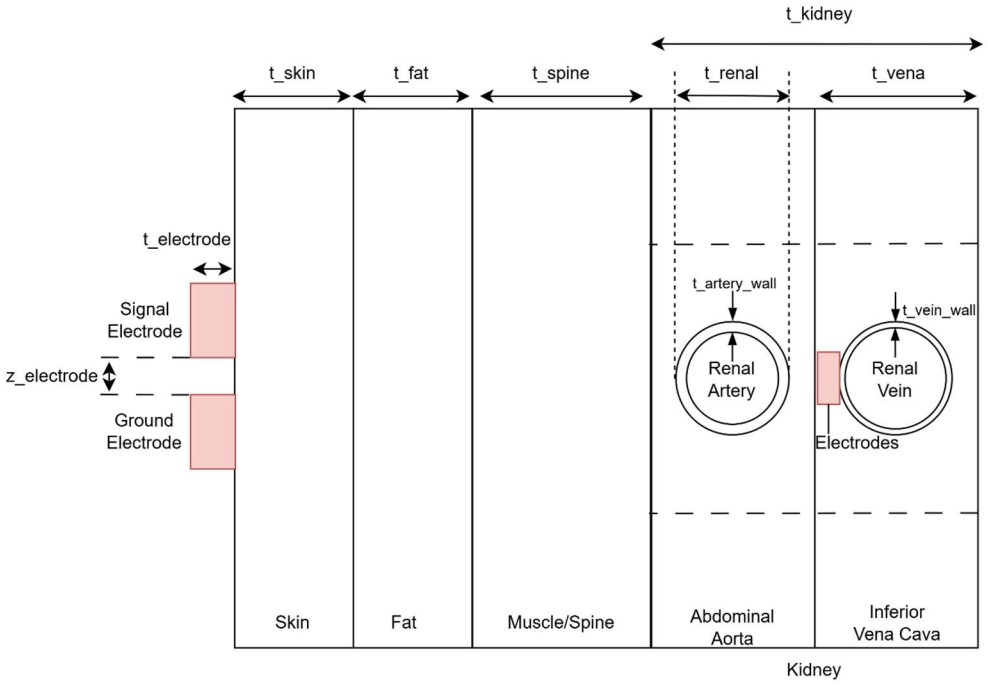

Figure 17: HBC Channel, CM4 Model Blueprint (Side-view).

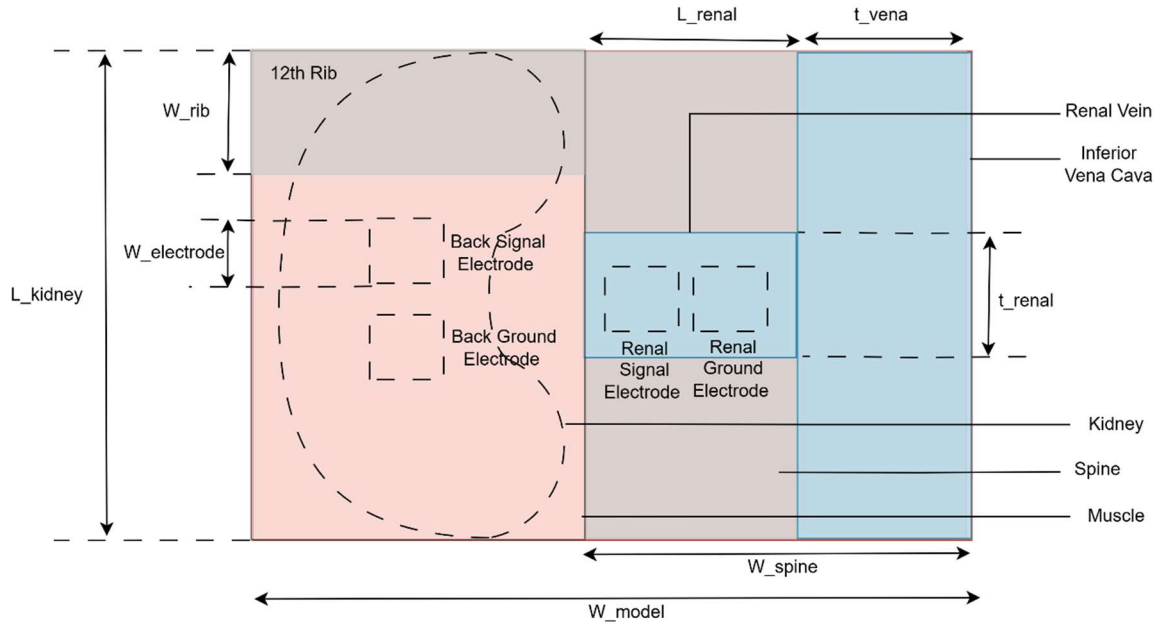

Figure 18: HBC Channel, CM4 Model Blueprint (Front-view).

Table 5: FEM Modelling Parameters for the Left Renal Vein to Kidney Channel.

Parameter	Value	Description
t_{kidney}	4 [cm]	Thickness of the left human kidney (Soriano, Penfold, and Leslie 2023).
t_{muscle}	2.87 [cm]	Thickness of the posterior muscles at the back of a human (Miyachi et al. 2022).
t_{fat}	4 [mm]	Thickness of the subcutaneous fat at the posterior trunk of a human (Störchle et al. 2018).
$t_{rib\_cancellous}$	0.9 [mm]	Thickness of the cancellous bone of the human rib (Holcombe et al. 2019).
t_{rib}	6 [mm]	Thickness of the human rib (Mohr et al. 2007).
t_{skin}	116 [um]	Thickness of the skin at the posterior trunk of a human (Oltulu et al. 2018).
t_{spine}	3.6 [cm]	Average thickness of the human spine (lumbar) (Zhou et al. 2000).
t_{renal}	8.9 [mm]	Average diameter of the left renal vein (Poyraz et al. 2013). This is assumed to be the diameter of the left renal artery.
t_{vena}	2.2 [cm]	Average diameter of the inferior vena cava (Cleveland Clinic Medical 2024b). This is assumed to be the diameter of the abdominal artery.
$t_{vein\ wall}$	0.5 [mm]	Average thickness of the renal vein wall (Tu and Chao 2018).

$t_{artery\ wall}$	1 [mm]	Average thickness of the renal vein wall (Tu and Chao 2018).
$t_{vena\ wall}$	1.5 [mm]	Average thickness of the inferior vena cava wall (Tu and Chao 2018).
$t_{abdomnial\ wall}$	2.0 [mm]	Average thickness of the abdominal aorta wall (Tu and Chao 2018).
L_{kidney}	11 [cm]	Length of the human kidney (Soriano, Penfold, and Leslie 2023).
L_{mid}	1 [cm]	Chosen for this study.
L_{renal}	6 [cm]	Length of the left renal vein (Cleveland Clinic Medical 2024a).
L_{spine}	5.31 [cm]	Average length of the human spine (lumbar) (Zhou et al. 2000).
W_{model}	19 [cm]	Width of CM4 area under study.
W_{kidney}	6 [cm]	Width of the human kidney (Soriano, Penfold, and Leslie 2023).
W_{rib}	11.3 [mm]	Width of the human rib (Mohr et al. 2007).

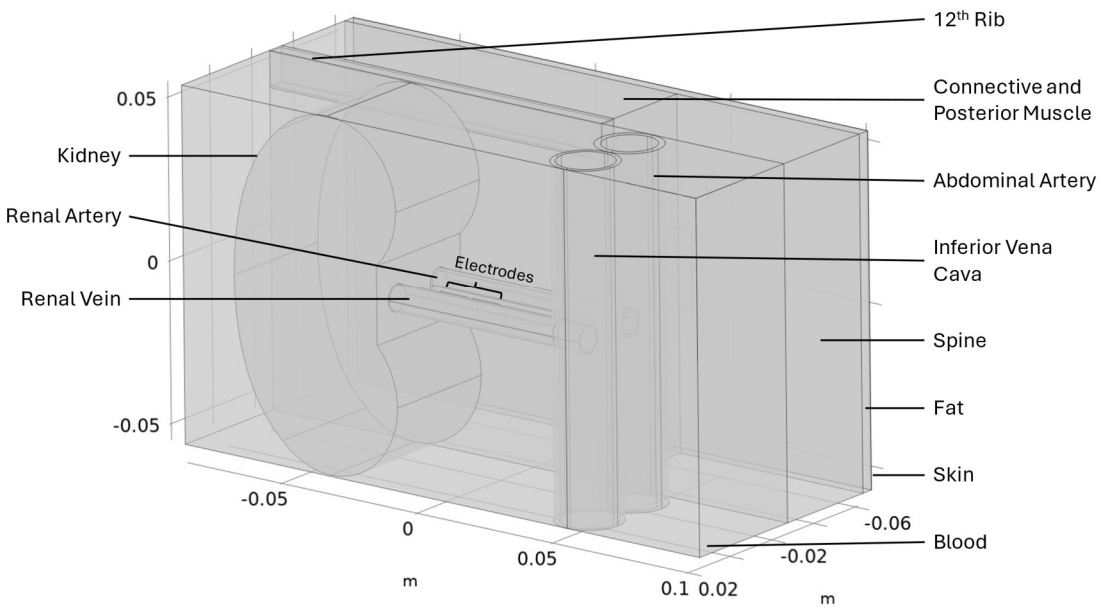

Figure 19: COMSOL Model for the Kidney to Back Model (CM4).

CM5: Left Renal Vein to Kidney

This channel model used a similar geometry presented previously to realize the communication pathway in Figure 5. The pair of renal electrodes are now in front of the renal vein and there is a pair of electrodes on the kidney rather than the back. Additionally, the fat and skin layers are removed as they are not between the transmitter and receiver electrodes. However, structures near the electrodes are retained such as the spine/muscle layer. These changes are observed in the model blueprints in Figure 20 and Figure 21. The relevant parameters detailed in Table 5 are used to realize this model in COMSOL. The renal vein electrodes are maintained 1 cm. Finally, the model blueprints and parameters are used to construct the COMSOL model in Figure 22

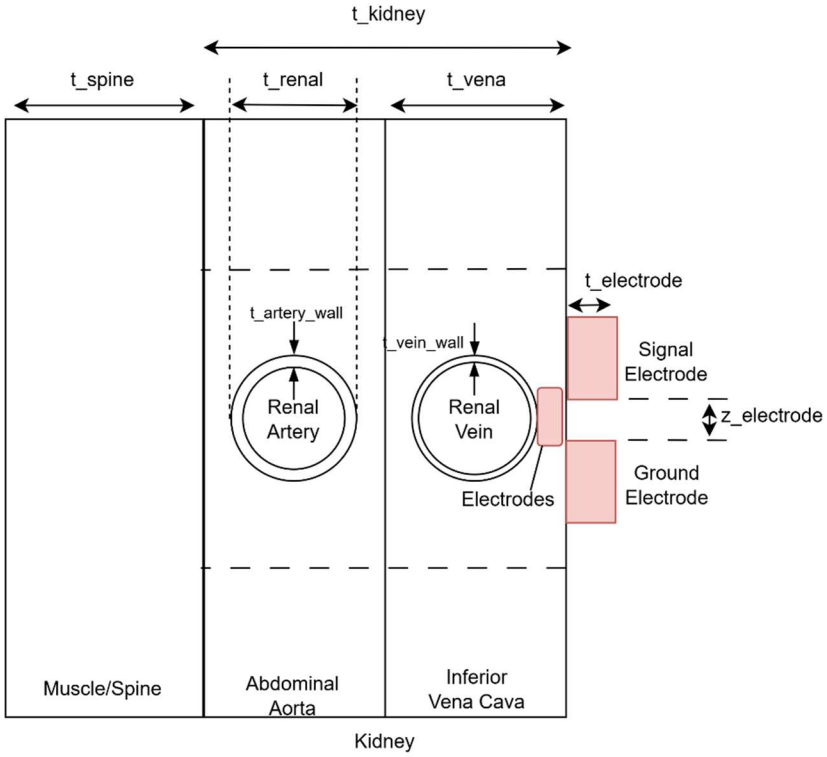

Figure 20: HBC Channel, CM5 Model Blueprint (Side-view).

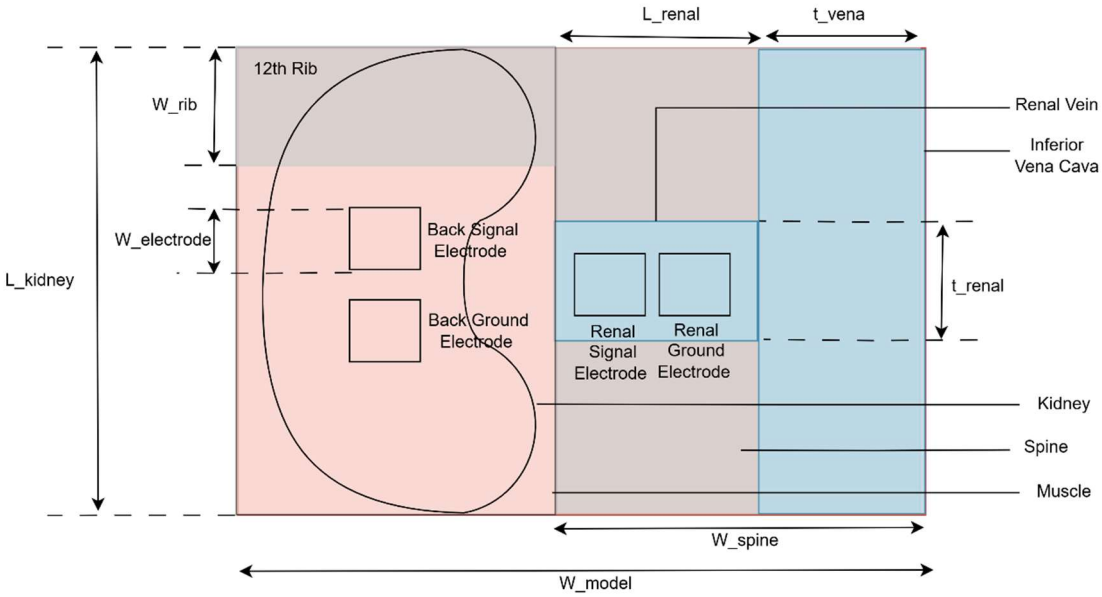

Figure 21: HBC Channel, CM5 Model Blueprint (Front-view).

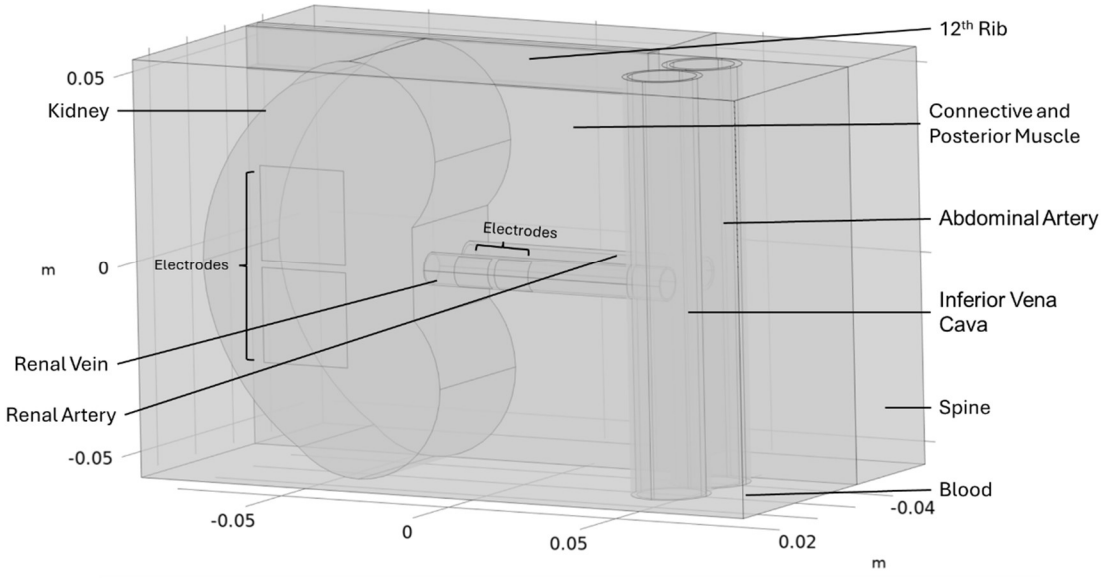

Figure 22: COMSOL Model for the Kidney to Renal Vein Model (CM5).

Bianco, Carl. 2021. “How Your Heart Works.” HowStuffWorks. February 11, 2021. https://health.howstuffworks.com/human-body/systems/circulatory/heart1.htm.

Callejon, Maria Amparo, David Naranjo-Hernandez, Javier Reina-Tosina, and Laura M. Roa. 2013. “A Comprehensive Study into Intrabody Communication Measurements.” *IEEE Transactions on Instrumentation and Measurement* 62 (9): 2446–55. https://doi.org/10.1109/TIM.2013.2258766.

Chekan, Edward G, John F Cummings, Isaac Mabe, Shawn Hunter, and Jeffrey W Clymer. 2016. “Thickness of Cadaveric Human Lung Tissue.” *Surgical Technology International* 29 (October):207–13.

Cleveland Clinic Medical. 2024a. “Renal Vein.” October 4, 2024.

———. 2024b. “Vena Cava.” May 1, 2024.

Davis, Anne, Cameron Holloway, Adam J Lewandowski, Ntobeko Ntusi, Richard M Nethononda, Alex Pitcher, Jane M Francis, Paul Leeson, Stefan Neubauer, and Oliver J Rider. 2013. “Diameters of the Normal Thoracic Aorta Measured by Cardiovascular Magnetic Resonance Imaging; Correlation with Gender, Body Surface Area and Body Mass Index.” *Journal of Cardiovascular Magnetic Resonance* 15 (January):E77. https://doi.org/10.1186/1532-429x-15-s1-e77.

Erbel, Raimund, and Holger Eggebrecht. 2006. “Aortic Dimensions and the Risk of Dissection.” *Heart*. https://doi.org/10.1136/hrt.2004.055111.

Filippi, Prof Simonetta, and Christian Cherubini. 2024. “Electrical Signals in a Heart.” www.comsol.com/trademarks.

Hacking, Craig, and Stefano Pacifici. 2011. “Pectoralis Major Muscle.” In *Radiopaedia.Org*. Radiopaedia.org. https://doi.org/10.53347/rID-15425.

Holcombe, Sven A, Yun-Seok Kang, Brian A Derstine, Stewart C Wang, and Amanda M Agnew. 2019. “Regional Maps of Rib Cortical Bone Thickness and Cross-Sectional Geometry.” https://doi.org/10.1111/joa.13045.

Kawel, Nadine, Evrim B. Turkbey, J. Jeffrey Carr, John Eng, Antoinette S. Gomes, W. Gregory Hundley, Craig Johnson, et al. 2012. “Middle-Aged and Older Subjects with Steady-State Free Precession Cardiac Magnetic Resonance the Multi-Ethnic Study of Atherosclerosis.” *Circulation: Cardiovascular Imaging* 5 (4): 500–508. https://doi.org/10.1161/CIRCIMAGING.112.973560.

Lobodzinski, S.M. 2010. “ECG Instrumentation: Applicationand Design.” In *Comprehensive Electrocardiology*. Springer, London. https://doi.org/https://doi.org/10.1007/978-1-84882-046-3_12.

Miyachi, Ryo, Nana Koike, Suzu Kodama, and Junya Miyazaki. 2022. “Relationship between Trunk Muscle Strength and Trunk Muscle Mass and Thickness Using Bioelectrical Impedance Analysis and Ultrasound Imaging.” *Bio-Medical Materials and Engineering* 33 (1): 31–40. https://doi.org/10.3233/BME-211218.

Mohr, Marcus, Eduard Abrams, Christine Engel, William B. Long, and Michael Bottlang. 2007. “Geometry of Human Ribs Pertinent to Orthopedic Chest-Wall Reconstruction.” *Journal of Biomechanics* 40 (6): 1310–17. https://doi.org/10.1016/j.jbiomech.2006.05.017.

Nösslinger, Hannes, Ewald Mair, Hermann Toplak, and Marlies Hörmann-Wallner. 2022. "Measuring Subcutaneous Fat Thickness Using Skinfold Calipers vs. High-Resolution B-Scan Ultrasonography in Healthy Volunteers: A Pilot Study." *Clinical Nutrition Open Science* 41 (February):19–32. https://doi.org/10.1016/j.nutos.2021.11.007.

Oltulu, Pembe, Bilsev Ince, Naile Kökbudak, Sidika Findik, and Fahriye Kiliç. 2018. "Measurement of Epidermis, Dermis, and Total Skin Thicknesses from Six Different Body Regions with a New Ethical Histometric Technique." *Turkish Journal of Plastic Surgery* 26 (2): 56–61. https://doi.org/10.4103/tjps.tjps_2_17.

Poyraz, Ahmet K., Fatih Firdolas, Mehmet R. Onur, and Ercan Kocakoc. 2013. "Evaluation of Left Renal Vein Entrapment Using Multidetector Computed Tomography." *Acta Radiologica* 54 (2): 144–48. https://doi.org/10.1258/ar.2012.120355.

Sasaki, Kensuke, Kanako Wake, and Soichi Watanabe. 2014. "Development of Best Fit Cole-Cole Parameters for Measurement Data from Biological Tissues and Organs between 1 MHz and 20 GHz." *Radio Science* 49 (7): 459–72. https://doi.org/10.1002/2013RS005345.

Soriano, Roberto M., Dana Penfold, and Stephen W. Leslie. 2023. "Anatomy, Abdomen and Pelvis: Kidneys." *StatPearls*, July. https://www.ncbi.nlm.nih.gov/books/NBK482385/.

Störchle, Paul, Wolfram Müller, Marietta Sengeis, Sonja Lackner, Sandra Holasek, and Alfred Fürhapter-Rieger. 2018. "Measurement of Mean Subcutaneous Fat Thickness: Eight Standardised Ultrasound Sites Compared to 216 Randomly Selected Sites." *Scientific Reports* 8 (1). https://doi.org/10.1038/s41598-018-34213-0.

Tu, Tse-Yi, and Paul C.-P. Chao. 2018. “Continuous Blood Pressure Measurement Based on a Neural Network Scheme Applied with a Cuffless Sensor.” *Microsystem Technologies* 24 (11): 4539–49. https://doi.org/10.1007/s00542-018-3957-4.

Zhou, S. H., I. D. McCarthy, A. H. McGregor, R. R.H. Coombs, and S. P.F. Hughes. 2000. “Geometrical Dimensions ,of the Lumbar Vertebrae - Analysis of Data from Digitised CT Images.” *European Spine Journal* 9 (3): 242–48. https://doi.org/10.1007/S005860000140/METRICS.